Earth and Planetary Science Letters 562 (2021) 116854

Contents lists available at ScienceDirect

Earth and Planetary Science Letters

www.elsevier.com/locate/epsl

# Inverted channel belts and floodplain clays to the East of Tempe Terra, Mars: Implications for persistent fluvial activity on early Mars

Zhenghao Liu [a,b], Yang Liu [a,c,*], Lu Pan [d], Jiannan Zhao [e], Edwin S. Kite [f], Yuchun Wu [a,b], Yongliao Zou [a]

[a] State Key Laboratory of Space Weather, National Space Science Center, Chinese Academy of Sciences, Beijing 100190, China
[b] University of Chinese Academy of Science, Beijing 100049, China
[c] Center for Excellence in Comparative Planetology, Chinese Academy of Sciences, Hefei 230026, China
[d] University of Copenhagen, GLOBE Institute, Center for Star and Planet Formation, Denmark
[e] Planetary Science Institute, China University of Geosciences, Wuhan 430074, China
[f] University of Chicago, Chicago, IL 6063, USA

ARTICLE INFO

*Article history:*
Received 15 September 2020
Received in revised form 19 February 2021
Accepted 21 February 2021
Available online xxxx
Editor: W.B. McKinnon

*Keywords:*
early Mars
sinuous ridges
floodplain clays
fluvial activity
warming events

ABSTRACT

The climate on early Mars is one of the major unsolved problems in planetary science. It is unclear whether early Mars was warm and wet or cold and icy. Morphological features on Mars such as sinuous ridges could provide critical constraints to address this issue. Here we investigate several sinuous ridges to the east of Tempe Terra, located at the dichotomy boundary of the highland terrain and lowland plains and find these ridges may have recorded persistent fluvial activity on early Mars. Our analysis indicates that these ridges may represent exhumation of the channel belts and overbank deposits formed from meandering rivers over significant geologic time. Layered smectite-bearing minerals are distributed along the flank of the ridges, and could be detrital or authigenic floodplain clays. Our interpretation of the stratigraphic relationships indicates that the layered smectite-bearing materials lie between channel belt deposits, which has rarely been previously reported on Mars and supports the floodplain interpretation. Our results suggest a persistent warm period, perhaps triggered by volcanism, impacts, and/or variations in planetary obliquity, that persisted for a geologically significant interval (tens of thousands of years) during the Noachian period of Mars.



## 1. Introduction

The nature and evolution of the climate of early Mars (i.e., Noachian to early Hesperian) is a fascinating and fundamental, yet unsolved problem. Widely distributed clay minerals, as well as geomorphological features such as valley networks, alluvial fans, lake basins, and deltas, suggest the presence of liquid water and a persistent relatively warm and wet climate on early Mars (e.g., Craddock and Howard, 2002; Howard et al., 2005; Howard, 2007; Fassett and Head, 2008; Goudge et al., 2012; Mischna et al., 2013; Ramirez and Craddock, 2018). However, global climate modeling suggests Mars could have been cold and icy in the Noachian with only transient warm and wet periods (e.g., Wordsworth et al., 2015; Palumbo and Head, 2020), which could also explain the distribution of sedimentary rocks and other geomorphic observations (Kite et al., 2013a; Wordsworth, 2016). Geomorphic (Buhler et al., 2014; Lapôtre and Ielpi, 2020) and geochemical (Bishop et al., 2018) analysis of Martian terrains could provide critical information to test and constrain global climate models for early Mars. Of particular interest among Mars' geomorphological landforms are sinuous ridges. Sinuous ridges are widely distributed on the surface of Mars, showing a variety of ridge cross section types and lengths of tens to hundreds of kilometers (Burr et al., 2009; Williams et al., 2013; Dickson et al., 2020). Although some sinuous ridges on Mars were considered to be eskers (Banks et al., 2009; Butcher et al., 2016, 2017, 2020), many sinuous ridges may be composed of strata from fluvial depositional systems and could have recorded a prolonged aqueous history over millions of years (Hayden et al., 2019). Therefore, the analysis of sinuous ridges could provide important insight on climate conditions on early Mars.

Many sinuous ridges have been identified and analyzed on Mars (e.g., Banks et al., 2009; Williams et al., 2013; Dickson et al., 2020), however, it is much less common for hydrated minerals to be reported in association with sinuous ridges, except in one location

* Corresponding author.
*E-mail address:* yangliu@nssc.ac.cn (Y. Liu).

https://doi.org/10.1016/j.epsl.2021.116854
0012-821X/

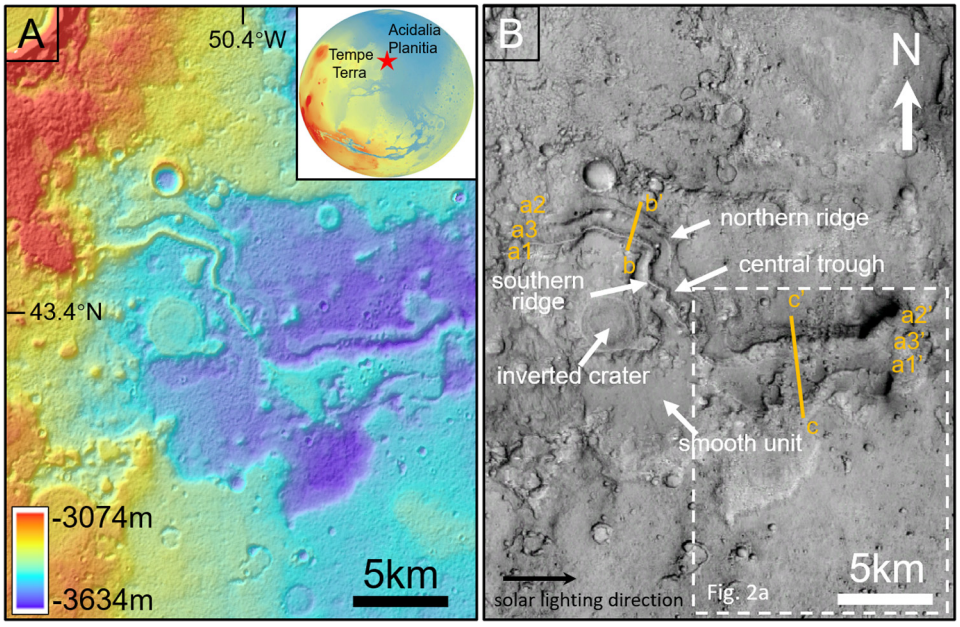


**Fig. 1.** (a) CTX DEM of the study area generated from images J19_052275_2237_XN_43N050W and J20_052552_2237_XN_43N050W. The inset on the top right is a Mars Orbiter Laser Altimeter (MOLA) global map where the study region is indicated by a red star. Parallel inverted sinuous ridges are evident in a topographic depression. (b) Geological context of the study area shown in the CTX image (J19_052275_2237_XN_43N050W) which has the same extent as panel A. (For interpretation of the colors in the figure, the reader is referred to the web version of this article.)

in Miyamoto crater, near the Opportunity landing site (Wiseman et al., 2008; Marzo et al., 2009; Newsom et al., 2010). In many terrains that contain valley networks, topographically inverted ridges have been reported in many terrains that contain valley networks, including Arabia Terra (Davis et al., 2019), Aeolis Dorsa/Medusae Fossae Formation (Lefort et al., 2012; Williams et al., 2013; Cardenas et al., 2018) and Miyamoto crater (Newsom et al., 2010), among other sites, providing evidence for prolonged fluvial activity in these areas. These sinuous ridges may represent exhumation of the channel belts and overbank deposits formed from meandering rivers over significant geologic time (DiBiase et al., 2013; Cardenas et al., 2018; Hayden et al., 2019). If this is the case, the sequence of fluvial floodplain and channel-belt deposits contained in these ridges may preserve markers of chemical alteration to form hydrated minerals (either in-situ or in upstream soils (Lapôtre et al., 2019)). However, it remains unclear whether channel-belt deposits in association with floodplain clays exist on Mars.

Here we report a detailed analysis of sinuous ridges, located to the east of Tempe Terra at the dichotomy boundary of Martian highlands and lowland plains (Fig. 1), which were previously noted by Pan and Ehlmann (2014). Tempe Terra is the northernmost exposure of ancient heavily cratered highland terrain and has a complex history (Tanaka et al., 2014). Tempe Terra grades into Acidalia Planitia to the east, connecting the old Noachian terrain to the smooth northern plains. Our study region lies in a stratigraphic context at the transition from the highland material in Tempe Terra to the lowlands of Acidalia Planitia (Fig. 1). These sinuous ridges show distinct geomorphology and are consistent with inverted channel belts and overbank deposits. The clay minerals associated with these inverted ridges are analyzed and their formation mechanisms are discussed. Finally, the inferred climatic conditions to form these sinuous ridges and clay minerals on early Mars are presented.

## 2. Data and methods

We used data from Mars Reconnaissance Orbiter (MRO) instruments, including the Context Camera (CTX), the High-Resolution Imaging Science Experiment (HiRISE), and the Compact Reconnaissance Imaging Spectrometer for Mars (CRISM). CTX images (spatial resolution of 5-6.5 m/pixel) (Malin et al., 2007) were used to examine the geological context of the ridges. HiRISE images (resolution up to 0.3 m/pixel) (McEwen et al., 2007), were used to examine the geomorphic details. Digital elevation models (DEM) were constructed from both CTX and HiRISE stereopairs, and were also utilized for quantitative analysis on the topography. The DEMs were generated using the NASA Ames Stereo Pipeline (ASP) (Broxton and Edwards, 2008; Moratto et al., 2010; Beyer et al., 2014; Shean et al., 2016). CRISM data with targeted mode (18-36 m/pixel, 362-3920 nm at 6.55 nm/channel) were processed with the volcano scan correction method and used to identify the type and distribution of minerals in the study area (Murchie et al., 2007; McGuire et al., 2009). To map the distribution of hydrated minerals, we applied the spectral parameters of Viviano-Beck et al. (2014) using the band depths at 1.9 μm (BD1900R2, blue), 2.1 μm (BD2100_2, green), and the convexity at 2.29 μm due to the absorption at 1.9/2.1 μm & 2.4 μm (SINDEX2, red).

To better characterize the morphology of the sinuous ridges, we calculated both their flank slopes and the slope along a down-ridge topographic profile. To get the flank slope of the ridges, the height difference between the top and bottom of the ridges is divided by the half width of the bottom of the ridge. For the along-ridge bed slope, we use a sixth-order polynomial function to fit the longitudinal profiles taken along the crest of the ridge, and then we take the first derivative of this function to get the slope.

Crater size-frequency distribution (CSFD) measurements (Hartmann and Neukum, 2001; Ivanov, 2001; Neukum et al., 2001) were performed with CTX images to acquire the model ages of the sinuous ridges. Secondary craters such as crater chains and clusters were excluded in the crater counting.

## 3. Results

Two sinuous and parallel ridges are evident in the CTX DEM map (Fig. 1a). The geologic context of these ridges is shown in Fig. 1b. The ridges are 30-35 km long, extending down slope to the

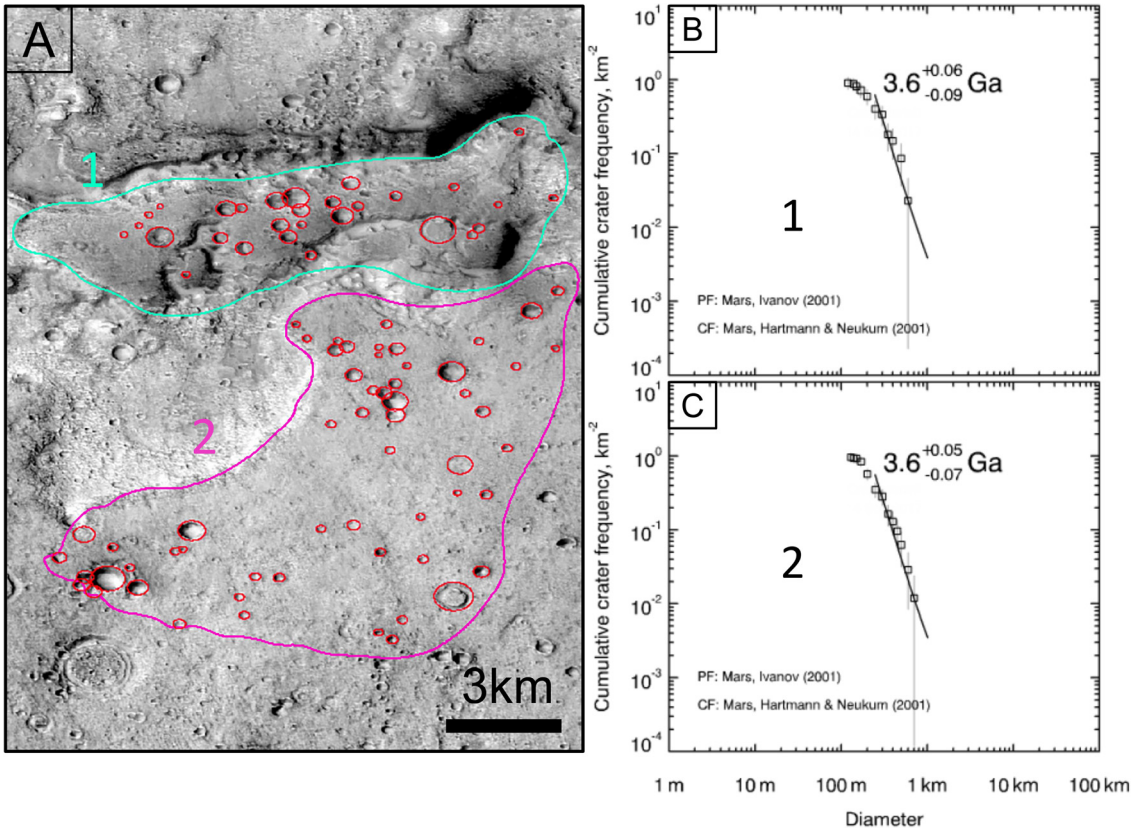


**Fig. 2.** (a) CTX image of the areas used to perform crater counting analysis are outlined with green and red lines, respectively. Craters counted are outlined with red circles. The location of the area is indicated in Fig. 1b. (b, c) The crater size-frequency distributions and absolute model ages of the areas 1 and 2 outlined in panel A. (For interpretation of the colors in the figure, the reader is referred to the web version of this article.)

east at the boundary between the highland terrain and the lowland plains. The ridges are 50-60 m in height with a flank slope between ~8° and ~14°, superposing relatively old terrain (middle to late Noachian, (Tanaka et al., 2014)). Crater counting was performed over the part of the crest of the southern ridge and the surrounding area, and our CSFD analysis shows that the sinuous ridges have an early Hesperian age of ~3.6 Ga (Fig. 2). An inverted impact crater is observable to the southwest of the southern ridge, indicating the area has experienced extensive exhumation and denudation (Fig. 1b). The smooth unit to the southeast of the inverted crater represents a resurfacing event that may have filled the previous topography with lava or sediments (Fig. 1b).

The mineralogy associated with the sinuous ridges was investigated using CRISM data. Consistent with an earlier study (Pan and Ehlmann, 2014), we found the hydrated minerals are continuously distributed along both sides of the southern ridge as well as in various settings close to the ridge (Fig. 3a). The CRISM parameter maps were co-registered with the HiRISE and CTX DEM using manually picked ground control points to map the stratigraphic relationships of hydrated minerals and other units (Fig. 3b), which clearly shows that the hydrated mineral unit is located at the upper part of the talus slope, parallel to the capping unit of the ridge. The hydrated minerals show a combination of absorptions at 1.4 μm, 1.9 μm, and 2.3 μm, which are mostly consistent with Fe/Mg smectites (Fig. 4). Fe/Mg smectites show typical absorptions at 1.4 μm due to $H_2O$ and metal-OH vibrations, at 1.9 μm due to $H_2O$, and at 2.3 μm due to Fe/Mg-OH. The Fe and Mg endmembers of the smectite group have slightly different band centers around 1.4 and 2.3 μm (Ehlmann et al., 2009). The CRISM spectra are mostly centered at 1.39 and 2.31 μm (Fig. 4), indicating the materials are most likely a Mg-rich smectite such as saponite.

We show the HiRISE DEM perspective views of representative clay exposures on the flank of the sinuous ridges at Zone I (Fig. 4c), Zone II (Fig. 4d) and on the slope of a small butte to the south of ridges (Fig. 4e). At Zone I, apparently fine-grained layers with different thicknesses below the light-toned caprock (LTC) are visible, and the clay-bearing bedrock is mostly associated with the mid-toned and the lower dark-toned layers (MTL & LDTL) which are below the LTC and the dark-toned layer (DTL) (Fig. 4c). Clay detections are also evident within the lower and thick mid-toned layer (LMTL), immediately below the LDTL unit. The clay-bearing bedrock at Zone II and on the slope of the small butte to the south of the sinuous ridges is light-toned, and the texture of these outcrops is much rougher compared to Zone I (Fig. 4d and 4e). Eolian ripples and debris are evident immediately beneath these light-toned deposits, masking the contact with the underlying unit.

Interestingly, the smectites are found on the flanks of the southern ridge while no hydrated minerals were detected on the northern ridge. The topographic profiles along the two ridges and the channel show decreased elevation to the east (Fig. 5a). The along-ridge bed slope and width measurements at ~1000 m intervals along the ridge length of the southern ridge are plotted in Fig. 5b, indicating a steeper slope and smaller widths of the ridges at Zone I as compared to Zone II. The cross sections of the Zone I and Zone II of the two ridges are shown in Fig. 5c and 5d, respectively, both showing the southern ridge is much higher than the northern ridge. Because the horizontal offset between the ridges is only 1-2 km, the long-baseline slopes of the ridges are very gentle (average <0.5°, Fig. 5a), and there is no evidence for faulting at this site, we believe topographic elevation is a proxy for stratigraphic position. In turn, this suggests that the caprock material of the northern ridge stratigraphically predates the materials of the southern ridge, and that the clay-bearing material in the

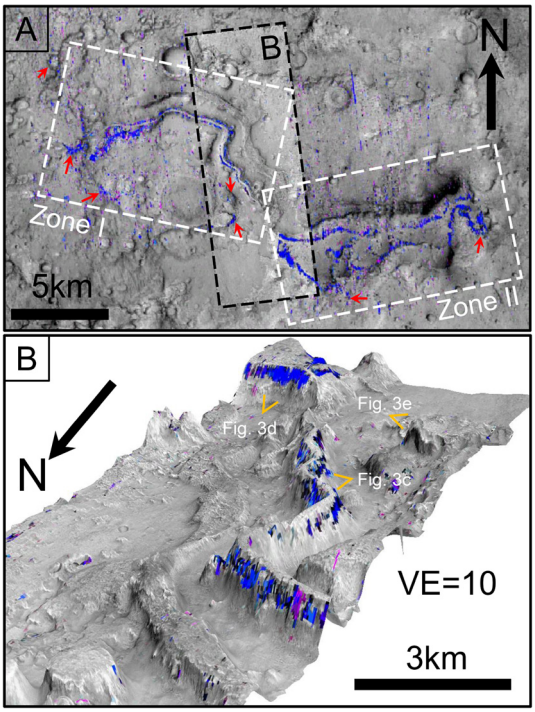


**Fig. 3.** (a) CRISM parameter map overlain on the CTX (J20_052552_2237_XN_43N050W) and HiRISE (ESP_052275_2235_RED) images. Areas with hydrated mineral signatures are indicated by blue to purple color. The ridges were divided into Zone I and II based on the different widths of the southern ridge. The hydrated minerals are distributed on both sides of the ridge flanks. These materials are also exposed in various settings close to the ridge, indicated by the red arrows. (b) HiRISE DEM image generated from HiRISE stereopair ESP_052275_2235_RED/ESP_052552_2235_RED. The hydrated minerals are distributed on both sides of the ridge flanks. Orange symbols show the locations and the approximate viewing directions for the perspective HiRISE views in Fig. 4c-e. A vertical exaggeration (VE) of 10 was used in the 3D visualization of the DEM. (For interpretation of the colors in the figure, the reader is referred to the web version of this article.)

southern ridge is stratigraphically encapsulated by episodes of deposition of material that formed sinuous-ridge caprock (Fig. 5c-d). This pattern, with sinuous deposits of erosionally-resistant materials bracketing clay-bearing, fine-grained erosionally recessive material, is also seen in terrestrial river-and-floodplain deposits (Bridge, 2003). This pattern has not previously been reported on Mars. It is possible that the northern ridge has similar clay mineral deposits beneath the capping unit, but that they are not visible due to differences in erosion and/or mass-wasting. Alternatively, clay may have never been formed at the location of the northern ridge. The topographic cross sections of Zone I and Zone II show that the ridges have flat-topped crests, and the surfaces of ridges for Zone II are rougher especially for the southern ridge due to cratering processes (Fig. 5c and 5d). The cross section also shows that the ~20-m thick clay-bearing unit underlies the caprock unit for the southern ridge, whereas the northern ridge lacks such a clay-bearing unit. The exposed clay-bearing strata sit along the cliff-forming caprocks and ridges (Fig. 3b), suggesting that significant erosion of side slopes has occurred (Wiseman et al., 2008; DiBiase et al., 2013; Hayden et al., 2019).

## 4. Discussion

Several interpretations have been proposed for sinuous ridges on Mars, including lava tubes, eskers, inverted channels, and inverted channel belts (Pain et al., 2007; Newsom et al., 2010; Lefort et al., 2012; Williams et al., 2013; Butcher et al., 2016; Bleacher et al., 2017; Butcher et al., 2017; Zhao et al., 2017; Cardenas et al., 2018; Davis et al., 2019; Hayden et al., 2019; Butcher et al., 2021). Lava tubes are mostly associated with volcanic activities and lava flows. Lava tubes or other magmatic intrusions could also explain the formation of smectite-bearing clay minerals underneath the capping unit through contact metamorphism; however, the observed morphology of the sinuous ridges is not consistent with such a formation scenario because of the lack of axial cracks or inflation clefts on the crest and the high sinuosity of the ridges (Zhao et al., 2017). Subglacial streams, consisting of glacial meltwater, will bring and deposit the sediments and form an esker. Smectite-bearing clay minerals could be formed during this process. However, there is strong evidence for exhumation and landscape inversion (e.g., the exhumed impact crater) and little evidence for glacial activities within the topographic depression, disfavoring an esker origin.

The inverted channel hypothesis has been widely used to explain the sinuous ridges observed on Mars (Williams et al., 2013). In this model, deposits fill the geometry of the paleo-channel to form a series of sedimentary materials, and a layer of caprock is formed through armoring, lithification, and/or cementation, which defines the erosion resistant materials on the riverbed (Williams et al., 2013, 2018). After deposition, burial, and channel abandonment, deposits would undergo weathering and erosion. Because the riverbed is covered with a layer of erosion-resistant caprock, it erodes at a slower pace than its surroundings. Over time, the riverbed will be raised and become a ridge (Pain et al., 2007; Zaki et al., 2018). Williams et al. (2013) proposed that the double ridges identified in Aeolis Serpens could have formed through either differential erosion of variably cemented deposits or the preservation of coarse-grained channel levees. These mechanisms could potentially explain the parallel ridges observed in our study area. However, there are some morphological differences between the double ridges observed in Aeolis Serpens and our site. For example, the two parallel ridges in Aeolis Serpens have similar height (i.e., <10 m), in contrast, the height difference for the two parallel ridges in our site is up to ~50 m. The bigger difference in ridge height may not be consistent with the differential cementation/erosion or the preservation of coarse-grained channel levee model. More terrestrial analog studies are needed to test these mechanisms.

An alternative explanation of the inverted sinuous ridge observed in the study area is an inverted channel belt (Fig. 6). An inverted channel belt represents the exhumed landform reflecting the lateral migration of rivers and vertical aggradation of river deposits rather than the original channel geometry (Mohrig et al., 2000; DiBiase et al., 2013; Hayden et al., 2019). The repeated flooding and deposition will form a channel belt sandstone body that is wider than the width of the river itself (Lapôtre and Ielpi, 2020). In addition, during the migration of the river, floodwater will overflow the riverbank and sediments will be transported to the floodplain. During exhumation, the elevation of the channel belt sandstone will be raised to form the ridge terrain due to the protection of the caprock and the channel fills may not be preserved, and late erosion would reduce the ridge width by lateral backwasting of the channel belt sandstone (Hayden et al., 2019).

The sinuous ridges observed in our study area are consistent with the inverted channel belt model of Hayden et al. (2019). A river floodplain forms where a meandering river floods the surrounding flat area and deposits the fine river sediments, and river channel migration and aggradation forms the channel belt. A flank slope of <15° are well below angle of repose slope (Ewing et al., 2017), which indicates mechanically weak materials, supporting the muddy floodplain hypothesis. The topographic profiles of the ridges show that the river was flowing from west to east following the dichotomy slope (Fig. 5a). The ridges (i.e., the southern ridge) at the flatter downstream area (i.e., Zone II; flat-crest top is ~1000-3000 m wide) are much wider but less steep than that at

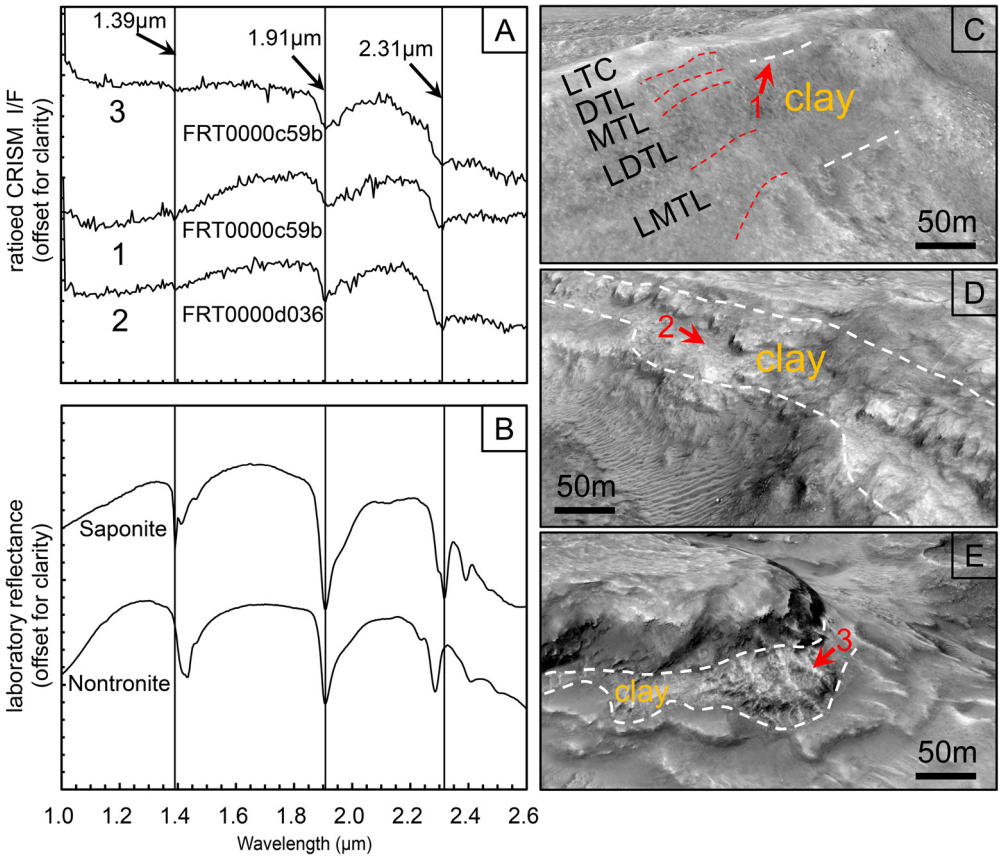


**Fig. 4.** (a) Ratioed CRISM I/F spectra (spectra with hydrated mineral signatures ratioed over the bland spectra lacking spectral features in a similar column in the image) of locations 1, 2, and 3, shown with red arrows in panels c–e. The spectra show absorption bands at 1.91 and 2.31 μm, with weak absorption features at 1.4 μm. (b) Laboratory spectra of saponite and nontronite from Reflectance Experiment Laboratory (RELAB, a NASA multiuser spectroscopy facility) in Brown University. The band positions of hydrated minerals in our study area are mostly consistent with those of saponite. (c-e) HiRISE orthorectified images overlain on the DEMs, showing perspective views of clay mineral-bearing exposures on the flank of the sinuous ridges at Zone I and Zone II and on the slope of a small butte to the south of the ridges, respectively. The vertical exaggeration of 3 was used in these scenes. The locations of these DEMs are indicated in Fig. 3b. LTC = light-toned caprock; DTL = dark-toned layer; MTL = mid-toned layer; LDTL = lower, dark-tone layer; LMTD = lower, mid-tone layer. (For interpretation of the colors in the figure, the reader is referred to the web version of this article.)

the upstream area (i.e., Zone I; flat-crest top is ~50-200 m wide) (Fig. 5b-d), suggesting that they may represent channel-belt deposits. During the formation of channel belts in fluvial systems, sediments can be deposited in association with lateral channel migration (Bridge, 2003; Willis and Tang, 2010; Ghinassi et al., 2016). In areas with gentle slopes such as the downstream of our study area (Fig. 5b), the channel belts could be wider due to more extensive lateral migration (Fig. 3a). Our model is similar to that of Cardenas et al. (2018), however, the sinuous ridges in our model were interpreted to be the remnants of channel belts that record the migration and aggradation of the river, which does not necessarily include any inverted channel fills.

The parallel northern ridge could be a locally indurated floodplain element, which would have been strengthened by some process producing a front that paralleled the channel belt (i.e., the southern ridge). These potential processes include chemical/weathering fronts extending from the channel outward into the floodplains, or even a thawed talik forming around a river channel in an frozen ground. Alternatively, the parallel northern ridge could also be an inverted channel belt. Detailed examination of HiRISE anaglyph image shows that in some areas the two ridges deviate from strict parallelism and tend to come close to intersecting, but at different topographic levels (Fig. 7). For example, a relatively well preserved local high on the top of the northern ridge is evident (marked with white dashed line, Fig. 7b), which is about the same width as the flat top on the southern ridge and may represent the course of a paleochannel, and some segments on the southern ridge (marked with white solid lines) trend at an azimuth very different from that of the northern ridge. Also, a possible constant-width, flat-topped ridge (outlined with gray line, Fig. 7c) is seen eroding out from underneath the southern ridge, which might correspond to the course of a paleochannel. This ridge apparently is not the same as the channel deposit from the southern ridge, which adds additional evidence for our multiple-channel-deposits-within-a-floodplain interpretation. Therefore, the two channel-belt deposits probably record rivers that formed at different times, with the lower-elevation channel-belt deposits (i.e., the northern ridge) forming first. The preferred stratigraphic interpretation is shown in Fig. 8. By analogy to terrestrial river-and-floodplain deposits (Bridge, 2003; Lapôtre et al., 2019; Lapôtre and Ielpi, 2020; Salese et al., 2020), which record frequent channel avulsions, these two distinct deposits might record intervals in the history of a single river.

Layered smectite-bearing clay minerals are distributed along both sides of the southern ridge flanks at the same stratigraphic level (Fig. 3b), which could correspond to the mudstone and sandstone of the floodplain. Indeed, the smectite-bearing clay minerals are not only distributed on the ridge slope, but also exposed in various settings as a continuous layer of phyllosilicates close to the ridge (Fig. 3a), indicating the possible wide distribution of the clay minerals in the floodplain, consistent with the formation and stability of a meandering river system (Lapôtre et al., 2019). These clay minerals could have been transported to their current location from the topographically higher surrounding plains, which would imply clay mineral-bearing source units for the detrital sediments (Milliken and Bish, 2010; Goudge et al., 2015). However, we sur-

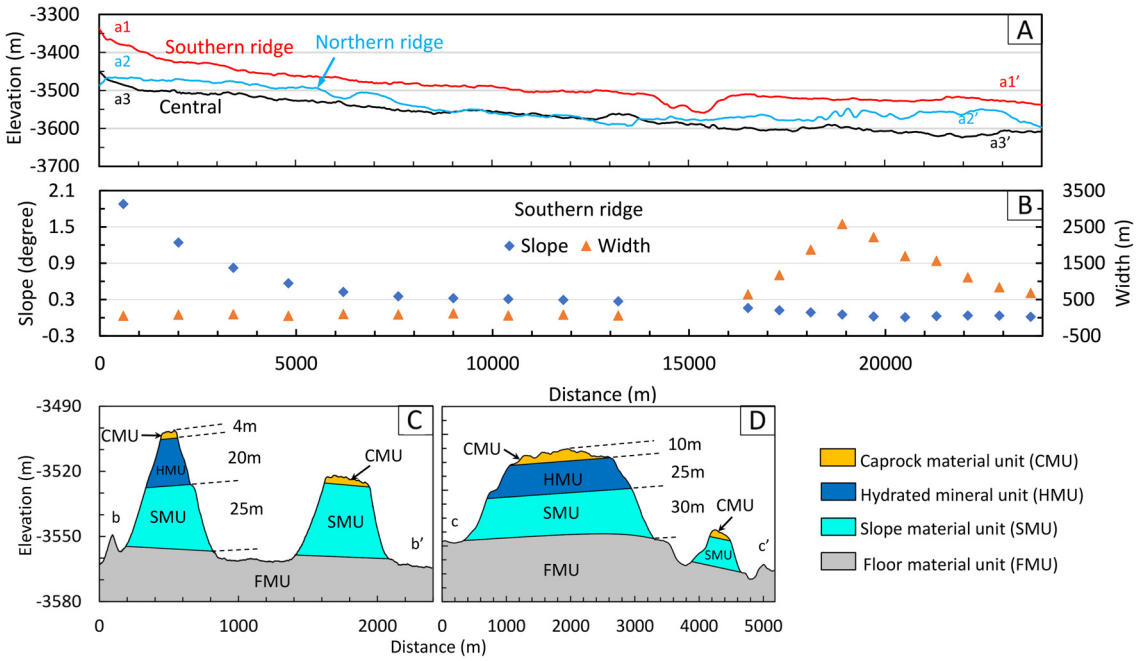


**Fig. 5.** (a) Topographic profiles: longitudinal profiles taken along the crest of the southern ridge (a1-a1'), the crest of the northern ridge (a2-a2'), and the trough in the middle (a3-a3'). (b) Plot of the slope along a down-ridge topographic profile and width measurements at ~1000 m intervals along the ridge length of the southern ridge. (c) Cross-sectional profile of the ridges in Zone I. Cross-sectional profile of the ridges in Zone II. The geologic units across the ridges in Zone I and II include: caprock material unit (CMU), hydrated mineral unit (HMU), slope material unit (SMU) and the floor material unit (FMU). The locations of the profiles of a1-a1', a2-a2', and a3-a3' in panel A, b-b' in panel C, and c-c' in panel D are indicated in Fig. 1b. (For interpretation of the colors in the figure, the reader is referred to the web version of this article.)

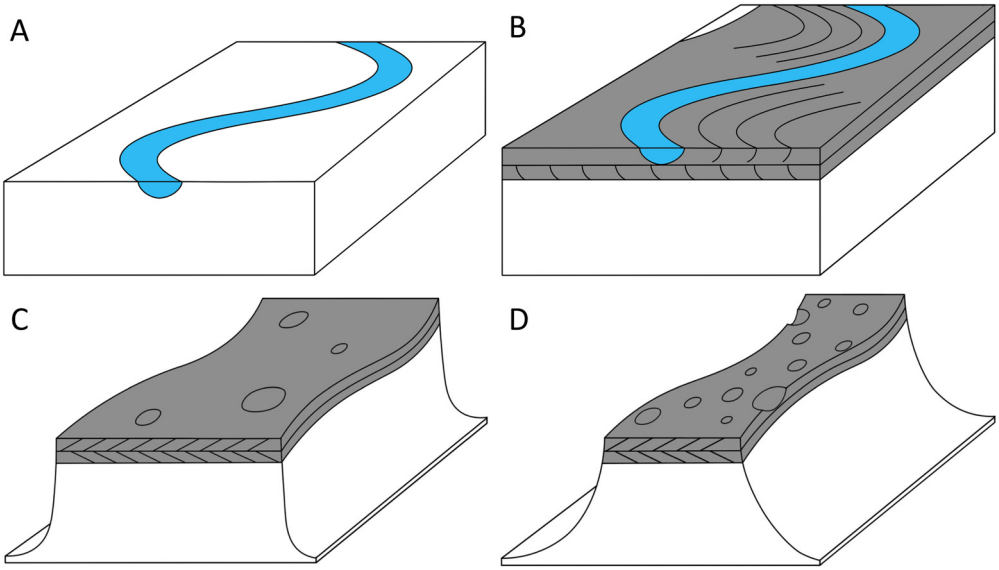


**Fig. 6.** Interpreted formation process of the sinuous ridges observed in the study area. (a) A active river flows across the surface of Mars, (b) The river aggrades and migrates across the floodplain and generates a layer of sediments on the floodplain, (c) Exhumation of the channel belts and overbank deposits has formed the initial stage of the sinuous ridge (dark circles represent craters), where the original channel and channel fills have been eroded and disappeared, (d) Under long-term weathering, the channel-belt has formed a ridge-like terrain with varying width. (For interpretation of the colors in the figure, the reader is referred to the web version of this article.)

veyed the potential source regions to the west of our study area and did not find widespread exposures of clay minerals. Although it is possible that some local clay deposits exist in the source region but are concealed by dust, the absence of large outcrops suggest that the clay minerals are likely not detrital, but authigenic in origin, as is inferred for clays detected at Gale crater by the Curiosity rover. Alternatively, fine-grained materials such as ash or wind-blown sand/dust were transported to the area by wind during a period with less runoff and were then altered to form clay minerals by in situ pedogenesis (Le Deit et al., 2012; Carter et al., 2015; Loizeau et al., 2018). In this case, river flow reworked the wind-blown materials. In Miyamoto crater, on the dichotomy near Arabia Terra, clay minerals have also been found to be associated with the sinuous ridges, and similarly to our site, these clay minerals are distributed along the slope of the ridges as well as on the crater floor (Wiseman et al., 2008; Newsom et al., 2010). The clay minerals in Miyamoto crater were interpreted to be formed by either upstream alteration followed by detrital transport, or *in situ* alteration by fluvial activities. Sinuous ridges are widely distributed at the dichotomy boundary on Mars (Lefort et al., 2012), and the processes to form the sinuous ridge - clay mineral association may not be uncommon at the dichotomy boundary. Future robotic mis-

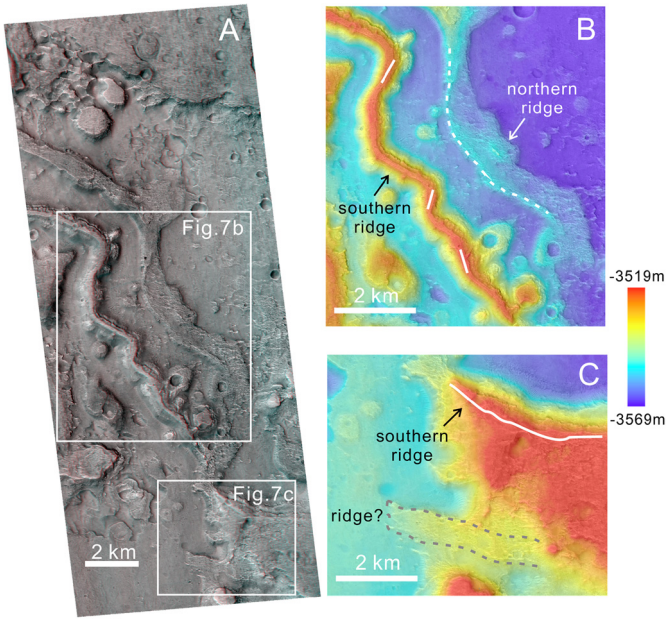


**Fig. 7.** (a) Anaglyph produced from HiRISE observations ESP_052552_2235 and ESP_052275_2235, showing nearly parallel northern and southern ridges. (b) HiRISE DEM showing areas where the southern ridge (marked with three white solid lines) that trend at an azimuth very different from that of the northern ridge. The white dash line marks the well preserved local high on the top of the northern ridge. (c) HiRISE DEM showing a possible ridge that erodes out from underneath the southern ridge, as outlined by gray dash line. (For interpretation of the colors in the figure, the reader is referred to the web version of this article.)

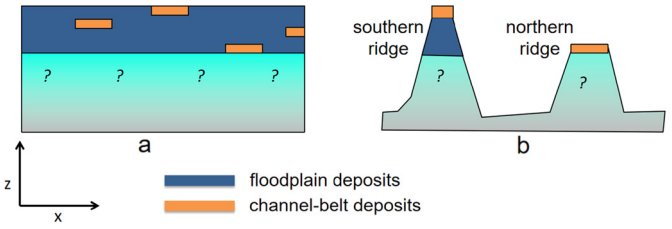


**Fig. 8.** The preferred stratigraphic interpretation on the formation of the southern and the northern ridges. (a) Formation of floodplain deposits and channel-belt deposits. Rivers that formed at different times meander over and flood a relatively flat area to form these deposits. (b) Formation of the southern and the north ridges. During exhumation, the elevation of the channel belt sandstone will be raised to form the ridge terrain due to the protection of the caprock, and the two ridges correspond to channel-belt deposits that formed at different times. (For interpretation of the colors in the figure, the reader is referred to the web version of this article.)

sions, such as the ExoMars Rosalind Franklin rover, planned to land in the Oxia Planum region near the dichotomy (Quantin-Nataf et al., 2021), may determine whether the origin of these clay minerals is detrital or authigenic.

The inverted channel belts and the associated clay minerals deposited on the channel belts and the floodplain identified in this study have important implications for the aqueous history of the region. The inverted ridges are located on mid-late Noachian terrain, around Mars' dichotomy boundary where valley networks terminate in deltas that may have formed along the coastline of an putative ancient ocean in northern lowlands (Parker et al., 1989; Rodriguez et al., 2016; Fawdon et al., 2018) although the northern ocean hypothesis is still debated (Rivera-Hernandez and Palucis, 2019). Crater counting analysis indicates the sinuous ridges have an age of ~3.6 Ga (Fig. 2), suggesting an active fluvial system no later than early Hesperian. A major open question is the duration of fluvial deposition and flow intermittency (e.g., Buhler et al., 2014; Lapôtre and Ielpi, 2020) at this proposed paleo-ocean shoreline. The thick clay-bearing layer (~20 m) on the flank of the 30 km long inverted channel belt and the widespread distribution of clay minerals on the interpreted floodplain, stratigraphically bracketed by channel belt deposits, implies prolonged fluvial activity on early Mars. At long-term terrestrial floodplain aggradation rates, a thickness of ~30 m corresponds to a time interval of $1.5 \times 10^3$ – $9 \times 10^4$ yrs (Bridge and Leeder, 1979). This timescale could be much longer on Mars due to intermittency (Buhler et al., 2014; Lapôtre and Ielpi, 2020). The aggradation rate is a strong function of the hydrograph, sediment supply, and subsidence, none of which are constrained and all of which could have been very different on early Mars than they are on modern Earth (e.g., Lapôtre et al., 2019; Lapôtre and Ielpi, 2020). For comparison, Salese et al. (2020) interpret a fluvial sedimentary succession of similar thickness in the northwestern rim of the Hellas basin of Mars as having been deposited over a period exceeding $10^5$ yrs.

Our site is antipodal to the Gale-Aeolis-Zephyria region, therefore, adding more evidence for the proposed argument that the prolonged fluvial activity (Kite et al., 2013b, 2015; Dickson et al., 2020) is globally distributed. It has been debated whether the Noachian period on Mars is "warm and wet" or "cold and icy". The valley networks and open-basin lakes distributed on the southern highlands indicate abundant liquid water, suggesting a warm and wet scenario of the Mars climate in the Noachian (Ramirez et al., 2020). However, climate models of Mars indicate that Mars could have been cold and arid in the Noachian and the fluvial landforms on Mars' surface may have been formed by flows of liquid water supplied by transient melting of snow or ice deposits (Wordsworth et al., 2013, 2015). If Noachian Mars was overall cold and arid as predicted by some climate models (e.g., Wordsworth et al., 2013, 2015), then the inferred persistent fluvial activity would require episodic but prolonged warming events. Possible mechanisms to trigger warming events over timescales of tens of thousands of years include volcanism (Wordsworth et al., 2017), impacts (Haberle et al., 2019), and/or variations in planetary obliquity (Mischna et al., 2013).

## 5. Conclusion

We report the identification of a series of inverted ridges to the east of Tempe Terra on Mars. These inverted ridges are interpreted to have formed by exhumation of the channel belts and overbank deposits that were formed from sinuous rivers over significant geologic time, which may shed light on the complex history of erosion and river activity close to the shoreline of the proposed Northern paleo-ocean on Mars. The widespread occurrence of smectite-bearing clay minerals on the flank of the inverted channel belt and the interpreted floodplain suggest prolonged fluvial activity on early Mars, potentially for tens of thousands of years (or longer if intermittency is taken into account).

## CRediT authorship contribution statement

**Zhenghao Liu:** Data curation, Formal analysis, Investigation, Methodology, Writing – original draft, Writing – review & editing. **Yang Liu:** Conceptualization, Formal analysis, Funding acquisition, Investigation, Methodology, Project administration, Validation, Supervision, Writing – original draft, Writing – review & editing. **Lu Pan:** Formal analysis, Investigation, Writing – review & editing. **Jiannan Zhao:** Formal analysis, Investigation, Writing – review & editing. **Edwin S. Kite:** Formal analysis, Investigation, Writing – review & editing. **Yuchun Wu:** Formal analysis, Validation. **Yongliao Zou:** Investigation, Supervision, Writing – review & editing.

## Declaration of competing interest

The authors declare that they have no known competing financial interests or personal relationships that could have appeared to influence the work reported in this paper.

## Acknowledgements

We thank Jay Dickson from the Murray Laboratory at Caltech and Caleb Fassett from NASA Marshall Space Flight Center for providing the CTX DEM and MarsSI for the help with generating the HiRISE DEM products. We thank two anonymous reviewers and the Editor, for useful comments that improved the manuscript. We thank the CRISM, HiRISE, CTX, MOLA teams for making Mars data available in this project. All the data used in this research are available through the Planetary Data System (https://pds-geosciences.wustl.edu/). This work is supported by the Strategic Priority Research Program of Chinese Academy of Sciences (Grant No. XDB 41000000), The National Natural Science Foundation of China (42072337, 11941001), the pre-research project on Civil Aerospace Technologies No. D020101 and D020102 funded by China National Space Administration (CNSA), National Key Research and Development Project (2019YFE0123300), and the Beijing Municipal Science and Technology Commission (Z191100004319001).

## References

Banks, M.E., Lang, N.P., Kargel, J.S., McEwen, A.S., Baker, V.R., Grant, J.A., Pelletier, J.D., Strom, R.G., 2009. An analysis of sinuous ridges in the southern Argyre Planitia, Mars using HiRISE and CTX images and MOLA data. J. Geophys. Res. 114 (E9). https://doi.org/10.1029/2008je003244.

Beyer, R., Alexandrov, O., Moratto, Z., 2014. Aligning terrain model and laser altimeter point clouds with the Ames Stereo Pipeline. Lunar Planet. Sci. XLV, abstract 2902.

Bishop, J.L., Fairen, A.G., Michalski, J.R., Gago-Duport, L., Baker, L.L., Velbel, M.A., Gross, C., Rampe, E.B., 2018. Surface clay formation during short-term warmer and wetter conditions on a largely cold ancient Mars. Nat. Astron. 2 (3). https://doi.org/10.1038/s41550-017-0377-9.

Bleacher, J.E., Orr, T.R., de Wet, A.P., Zimbelman, J.R., Hamilton, C.W., Garry, W.B., Crumpler, L.S., Williams, D.A., 2017. Plateaus and sinuous ridges as the fingerprints of lava flow inflation in the Eastern Tharsis Plains of Mars. J. Volcanol. Geotherm. Res. 342. https://doi.org/10.1016/j.jvolgeores.2017.03.025.

Bridge, J., 2003. Rivers and Floodplains: Forms, Processes, and Sedimentary Record. Blackwell Publishing.

Bridge, J.S., Leeder, M.R., 1979. A simulation model of alluvial stratigraphy. Sedimentology 26 (5).

Broxton, M.J., Edwards, L.J., 2008. The Ames Stereo Pipeline: automated 3D surface reconstruction from orbital imagery. Lunar Planet. Sci. XXXIX, abstract 2419.

Buhler, P.B., Fassett, C.I., Head III, J.W., Lamb, M.P., 2014. Timescales of fluvial activity and intermittency in Milna Crater, Mars. Icarus 241. https://doi.org/10.1016/j.icarus.2014.06.028.

Burr, D.M., Enga, M.T., Williams, R.M.E., Zimbelman, J.R., Howard, A.D., Brennand, T.A., 2009. Pervasive aqueous paleoflow features in the Aeolis/Zephyria Plana region, Mars. Icarus 200 (1). https://doi.org/10.1016/j.icarus.2008.10.014.

Butcher, F.E.G., Conway, S.J., Arnold, N.S., 2016. Are the Dorsa Argentea on Mars eskers? Icarus 275. https://doi.org/10.1016/j.icarus.2016.03.028.

Butcher, F.E.G., Balme, M.R., Gallagher, C., Arnold, N.S., Conway, S.J., Hagermann, A., Lewis, S.R., 2017. Recent basal melting of a mid-latitude glacier on Mars. J. Geophys. Res., Planets 122 (12). https://doi.org/10.1002/2017je005434.

Butcher, F.E.G., Balme, M.R., Conway, S.J., Gallagher, C., Arnold, N.S., Storrar, R.D., Lewis, S.R., Hagermann, A., 2020. Morphometry of a glacier-linked esker in NW Tempe Terra, Mars, and implications for sediment-discharge dynamics of subglacial drainage. Earth Planet. Sci. Lett. 542, 116325. https://doi.org/10.1016/j.epsl.2020.116325.

Butcher, F.E.G., Balme, M.R., Conway, S.J., Gallagher, C., Arnold, N.S., Storrar, R.D., Lewis, S.R., Hagermann, A., Davis, J.M., 2021. Sinuous ridges in Chukhung crater, Tempe Terra, Mars: implications for fluvial, glacial, and glaciofluvial activity. Icarus 357, 114131. https://doi.org/10.1016/j.icarus.2020.114131.

Cardenas, B.T., Mohrig, D., Goudge, T.A., 2018. Fluvial stratigraphy of valley fills at Aeolis Dorsa, Mars: evidence for base-level fluctuations controlled by a downstream water body. Geol. Soc. Am. Bull. 130 (3–4). https://doi.org/10.1130/b31567.1.

Carter, J., Loizeau, D., Mangold, N., Poulet, F., Bibring, J.P., 2015. Widespread surface weathering on early Mars: a case for a warmer and wetter climate. Icarus 248. https://doi.org/10.1016/j.icarus.2014.11.011.

Craddock, R.A., Howard, A.D., 2002. The case for rainfall on a warm, wet early Mars. J. Geophys. Res., Planets 107 (E11), 5111. https://doi.org/10.1029/2001je001505.

Davis, J.M., Gupta, S., Balme, M., Grindrod, P.M., Fawdon, P., Dickeson, Z.I., Williams, R.M.E., 2019. A diverse array of fluvial depositional systems in Arabia Terra: evidence for mid-noachian to early Hesperian rivers on Mars. J. Geophys. Res., Planets 124 (7). https://doi.org/10.1029/2019je005976.

DiBiase, R.A., Limaye, A.B., Scheingross, J.S., Fischer, W.W., Lamb, M.P., 2013. Deltaic deposits at Aeolis Dorsa: sedimentary evidence for a standing body of water on the northern plains of Mars. J. Geophys. Res., Planets 118 (6). https://doi.org/10.1002/jgre.20100.

Dickson, J.L., Lamb, M.P., Williams, R.M.E., Hayden, A.T., Fischer, W.W., 2020. The global distribution of depositional rivers on early Mars. Geology. https://doi.org/10.1130/G48457.1.

Ehlmann, B.L., et al., 2009. Identification of hydrated silicate minerals on Mars using MRO-CRISM: geologic context near Nili Fossae and implications for aqueous alteration. J. Geophys. Res., Planets 114, E00d08. https://doi.org/10.1029/2009je003339.

Ewing, R.C., et al., 2017. Sedimentary processes of the Bagnold Dunes: implications for the eolian rock record of Mars. J. Geophys. Res., Planets 122 (12). https://doi.org/10.1002/2017je005324.

Fawdon, P., Gupta, S., Davis, J.M., Warner, N.H., Adler, J.B., Balme, M.R., Bell, J.F., Grindrod, P.M., Sefton-Nash, E., 2018. The Hypanis Valles delta: the last highstand of a sea on early Mars? Earth Planet. Sci. Lett. 500. https://doi.org/10.1016/j.epsl.2018.07.040.

Fassett, C.I., Head, J.W., 2008. Valley network-fed, open-basin lakes on Mars: distribution and implications for Noachian surface and subsurface hydrology. Icarus 198, 37–56.

Ghinassi, M., Ielpi, A., Aldinucci, M., Fustic, M., 2016. Downstream-migrating fluvial point bars in the rock record. Sediment. Geol. 334. https://doi.org/10.1016/j.sedgeo.2016.01.005.

Goudge, T.A., Head, J.W., Mustard, J.F., Fassett, C.I., 2012. An analysis of open-basin lake deposits on Mars: evidence for the nature of associated lacustrine deposits and post-lacustrine modification processes. Icarus 219, 211–229.

Goudge, T.A., Mustard, J.F., Head, J.W., Fassett, C.I., Wiseman, S.M., 2015. Assessing the mineralogy of the watershed and fan deposits of the Jezero crater paleolake system, Mars. J. Geophys. Res., Planets 120 (4). https://doi.org/10.1002/2014je004782.

Haberle, R.M., Zahnle, K., Barlow, N.G., Steakley, K.E., 2019. Impact degassing of H-2 on early Mars and its effect on the climate system. Geophys. Res. Lett. 46 (22). https://doi.org/10.1029/2019gl084733.

Hartmann, W.K., Neukum, G., 2001. Cratering chronology and the evolution of Mars. Space Sci. Rev. 96 (1–4). https://doi.org/10.1023/a:1011945222010.

Hayden, A.T., Lamb, M.P., Fischer, W.W., Ewing, R.C., McElroy, B.J., Williams, R.M.E., 2019. Formation of sinuous ridges by inversion of river-channel belts in Utah, USA, with implications for Mars. Icarus 332. https://doi.org/10.1016/j.icarus.2019.04.019.

Howard, A.D., Moore, J.M., Irwin, R.P., 2005. An intense terminal epoch of widespread fluvial activity on early Mars: 1. Valley network incision and associated deposits. J. Geophys. Res., Planets 110 (E12), E12s14. https://doi.org/10.1029/2005je002459.

Howard, A.D., 2007. Simulating the development of Martian highland landscapes through the interaction of impact cratering, fluvial erosion, and variable hydrologic forcing. Geomorphology 91 (3–4). https://doi.org/10.1016/j.geomorph.2007.04.017.

Ivanov, B.A., 2001. Mars/moon cratering rate ratio estimates. Space Sci. Rev. 96 (1–4). https://doi.org/10.1023/a:1011941121102.

Kite, E.S., Halevy, I., Kahre, M.A., Wolff, M.J., Manga, M., 2013a. Seasonal melting and the formation of sedimentary rocks on Mars, with predictions for the gale crater mound. Icarus 223 (1). https://doi.org/10.1016/j.icarus.2012.11.034.

Kite, E.S., Lucas, A., Fassett, C.I., 2013b. Pacing early Mars river activity: embedded craters in the Aeolis Dorsa region imply river activity spanned greater than or similar to (1-20) Myr. Icarus 225 (1). https://doi.org/10.1016/j.icarus.2013.03.029.

Kite, E.S., Howard, A.D., Lucas, A., Lewis, K.W., 2015. Resolving the era of river-forming climates on Mars using stratigraphic logs of river-deposit dimensions. Earth Planet. Sci. Lett. 420. https://doi.org/10.1016/j.epsl.2015.03.019.

Lapôtre, M.G.A., Ielpi, A., Lamb, M.P., Williams, R.M.E., Knoll, A.H., 2019. Model for the formation of single-thread rivers in barren landscapes and implications for pre-Silurian and Martian fluvial deposits. J. Geophys. Res., Earth Surf. 124 (12). https://doi.org/10.1029/2019jf005156.

Lapôtre, M.G.A., Ielpi, A., 2020. The pace of fluvial meanders on Mars and implications for the western delta deposits of Jezero crater. AGU Adv. 1 (2). https://doi.org/10.1029/2019AV000141.

Le Deit, L., Flahaut, J., Quantin, C., Hauber, E., Mege, D., Bourgeois, O., Gurgurewicz, J., Masse, M., Jaumann, R., 2012. Extensive surface pedogenic alteration of the Martian Noachian crust suggested by plateau phyllosilicates around Valles Marineris. J. Geophys. Res., Planets 117, E00j05. https://doi.org/10.1029/2011je003983.

Lefort, A., Burr, D.M., Beyer, R.A., Howard, A.D., 2012. Inverted fluvial features in the Aeolis-Zephyria Plana, western Medusae Fossae formation, Mars: evidence for post-formation modification. J. Geophys. Res., Planets 117, E03007. https://doi.org/10.1029/2011je004008.

Loizeau, D., Quantin-Nataf, C., Carter, J., Flahaut, J., Thollot, P., Lozac'h, L., Millot, C., 2018. Quantifying widespread aqueous surface weathering on Mars: the plateaus South of coprates chasma. Icarus 302. https://doi.org/10.1016/j.icarus.2017.11.002.

Malin, M.C., et al., 2007. Context camera investigation on board the Mars reconnaissance orbiter. J. Geophys. Res. 112 (E5). https://doi.org/10.1029/2006je002808.

Marzo, G.A., Roush, T.L., Lanza, N.L., McGuire, P.C., Newsom, H.E., Ollila, A.M., Wiseman, S.M., 2009. Association of phyllosilicates and the inverted channel in Miyamoto crater, Mars. Geophys. Res. Lett. 36 (11). https://doi.org/10.1029/2009gl038703.

McEwen, A.S., et al., 2007. Mars reconnaissance orbiter's high resolution imaging science experiment (HiRISE). J. Geophys. Res., Planets 112 (E5), E05s02. https://doi.org/10.1029/2005je002605.

McGuire, P.C., et al., 2009. An improvement to the volcano-scan algorithm for atmospheric correction of CRISM and OMEGA spectral data. Planet. Space Sci. 57 (7). https://doi.org/10.1016/j.pss.2009.03.007.

Milliken, R.E., Bish, D.L., 2010. Sources and sinks of clay minerals on Mars. Philos. Mag. 90 (17-18), 2293–2308. https://doi.org/10.1080/14786430903575132.

Mischna, M.A., Baker, V., Milliken, R., Richardson, M., Lee, C., 2013. Effects of obliquity and water vapor/trace gas greenhouses in the early martian climate. J. Geophys. Res., Planets 118 (3). https://doi.org/10.1002/jgre.20054.

Mohrig, D., Heller, P.L., Paola, C., Lyons, W.J., 2000. Interpreting avulsion process from ancient alluvial sequences: Guadalope-Matarranya system (northern Spain) and Wasatch formation (western Colorado). Geol. Soc. Am. Bull. 112 (12). https://doi.org/10.1130/0016-7606(2000)112<1787:Iapfaa>2.0.Co;2.

Moratto, Z.M., Broxton, M.J., Beyer, R.A., Lundy, M., Husmann, K., 2010. Ames stereo pipeline, NASA's open source automated stereogrammetry software. Lunar Planet. Sci. XLI, abstract 2364.

Murchie, S., et al., 2007. Compact reconnaissance imaging spectrometer for Mars (CRISM) on Mars reconnaissance orbiter (MRO). J. Geophys. Res., Planets 112 (E5), E05s03. https://doi.org/10.1029/2006je002682.

Neukum, G., Ivanov, B.A., Hartmann, W.K., 2001. Cratering records in the inner solar system in relation to the lunar reference system. Space Sci. Rev. 96 (1–4). https://doi.org/10.1023/a:1011989004263.

Newsom, H.E., et al., 2010. Inverted channel deposits on the floor of Miyamoto crater, Mars. Icarus 205 (1). https://doi.org/10.1016/j.icarus.2009.03.030.

Pain, C., Clarke, J., Thomas, M., 2007. Inversion of relief on Mars. Icarus 190 (2). https://doi.org/10.1016/j.icarus.2007.03.017.

Palumbo, A.M., Head, J.W., 2020. Groundwater release on early Mars: utilizing models and proposed evidence for groundwater release to estimate the required climate and subsurface water budget. Geophys. Res. Lett. 47 (8), e2020GL087230. https://doi.org/10.1029/2020gl087230.

Pan, L., Ehlmann, B., 2014. Geology of the eastern margin of Tempe Terra with implications for Mars dichotomy modifications. In: Eighth International Conference on Mars. Abstract 1273.

Parker, T.J., Saunders, R.S., Schneeberger, D.M., 1989. Transitional morphology in West Deuteronilus Mensae, Mars - implications for modification of the lowland upland boundary. Icarus 82 (1). https://doi.org/10.1016/0019-1035(89)90027-4.

Quantin-Nataf, C., Carter, J., Mandon, L., Thollot, P., Balme, M., Volat, M., et al., 2021. Oxia Planum – the landing site for the ExoMars "Rosalind Franklin" rover mission: geological context and pre-landing interpretation. Astrobiology 21 (3), 1–22. https://doi.org/10.1089/ast.2019.2191 (in press).

Ramirez, R.M., Craddock, R.A., 2018. The geological and climatological case for a warmer and wetter early Mars. Nat. Geosci. 11 (4). https://doi.org/10.1038/s41561-018-0093-9.

Ramirez, R.M., Craddock, R.A., Usui, T., 2020. Climate simulations of early Mars with estimated precipitation, runoff, and erosion rates. J. Geophys. Res., Planets 125 (3), e2019JE006160. https://doi.org/10.1029/2019je006160.

Rivera-Hernandez, F., Palucis, M.C., 2019. Do deltas along the crustal dichotomy boundary of Mars in the Gale crater region record a northern ocean? Geophys. Res. Lett. 46 (15). https://doi.org/10.1029/2019gl083046.

Rodriguez, J.A.P., et al., 2016. Tsunami waves extensively resurfaced the shorelines of an early Martian ocean. Sci. Rep. 6, 25106. https://doi.org/10.1038/srep25106.

Salese, F., McMahon, W.J., Balme, M.R., Ansan, V., Davis, J.M., Kleinhans, M.G., 2020. Sustained fluvial deposition recorded in Mars' Noachian stratigraphic record. Nat. Commun. 11 (1), 2067. https://doi.org/10.1038/s41467-020-15622-0.

Shean, D.E., Alexandrov, O., Moratto, Z.M., Smith, B.E., Joughin, I.R., Porter, C., Morin, P., 2016. An automated, open-source pipeline for mass production of digital elevation models (DEMs) from very-high-resolution commercial stereo satellite imagery. ISPRS J. Photogramm. Remote Sens. 116. https://doi.org/10.1016/j.isprsjprs.2016.03.012.

Tanaka, K.L., Robbins, S.J., Fortezzo, C.M., Skinner, J.A., Hare, T.M., 2014. The digital global geologic map of Mars: chronostratigraphic ages, topographic and crater morphologic characteristics, and updated resurfacing history. Planet. Space Sci. 95. https://doi.org/10.1016/j.pss.2013.03.006.

Viviano-Beck, C.E., et al., 2014. Revised CRISM spectral parameters and summary products based on the currently detected mineral diversity on Mars. J. Geophys. Res., Planets 119 (6). https://doi.org/10.1002/2014je004627.

Williams, R.M.E., Irwin, R.P., Burr, D.M., Harrison, T., McClelland, P., 2013. Variability in martian sinuous ridge form: case study of Aeolis Serpens in the Aeolis Dorsa, Mars, and insight from the Mirackina paleoriver, South Australia. Icarus 225 (1). https://doi.org/10.1016/j.icarus.2013.03.016.

Williams, R.M.E., Moersch, J.E., Fergason, R.L., 2018. Thermophysical properties of Martian fluvial sinuous ridges: inferences on "inverted channel" induration agent. Earth Space Sci. 5 (9). https://doi.org/10.1029/2018ea000402.

Willis, B.J., Tang, H., 2010. Three-dimensional connectivity of point-bar deposits. J. Sediment. Res. 80 (5–6). https://doi.org/10.2110/jsr.2010.046.

Wiseman, S.M., et al., 2008. Phyllosilicate and sulfate-hematite deposits within Miyamoto crater in southern Sinus Meridiani, Mars. Geophys. Res. Lett. 35 (19), L19204. https://doi.org/10.1029/2008gl035363.

Wordsworth, R., Forget, F., Millour, E., Head, J.W., Madeleine, J.B., Charnay, B., 2013. Global modeling of the early martian climate under a denser CO2 atmosphere: water cycle and ice evolution. Icarus 222 (1). https://doi.org/10.1016/j.icarus.2012.09.036.

Wordsworth, R., Kalugina, Y., Lokshtanov, S., Vigasin, A., Ehlmann, B., Head, J., Sanders, C., Wang, H., 2017. Transient reducing greenhouse warming on early Mars. Geophys. Res. Lett. 44 (2). https://doi.org/10.1002/2016gl071766.

Wordsworth, R.D., Kerber, L., Pierrehumbert, R.T., Forget, F., Head, J.W., 2015. Comparison of "warm and wet" and "cold and icy" scenarios for early Mars in a 3-D climate model. J. Geophys. Res., Planets 120 (6). https://doi.org/10.1002/2015je004787.

Wordsworth, R.D., 2016. The climate of early Mars. In: Jeanloz, R., Freeman, K.H. (Eds.), Annual Review of Earth and Planetary Sciences, vol. 44. Annual Reviews, Palo Alto, pp. 381–408.

Zaki, A.S., Pain, C.F., Edgett, K.S., Giegengack, R., 2018. Inverted stream channels in the Western Desert of Egypt: synergistic remote, field observations and laboratory analysis on Earth with applications to Mars. Icarus 309. https://doi.org/10.1016/j.icarus.2018.03.001.

Zhao, J., Huang, J., Kraft, M.D., Xiao, L., Jiang, Y., 2017. Ridge-like lava tube systems in southeast Tharsis, Mars. Geomorphology 295. https://doi.org/10.1016/j.geomorph.2017.08.023.